Nonlinear Analysis: Modelling and Control, Vol. 22, No. 3, 421–429 ISSN 1392-5113
https://doi.org/10.15388/NA.2017.3.10

Inhibition of spikes in an array of coupled FitzHugh–Nagumo oscillators by external periodic forcing

Elena Adomaitienė[a], **Gytis Mykolaitis**[b], **Skaidra Bumelienė**[a], **Arūnas Tamaševičius**[a]

[a]Department of Electronics, Center for Physical Sciences and Technology, Saulėtekio ave. 3, LT-10223 Vilnius, Lithuania
elena.tamaseviciute@ftmc.lt; skaidra.bumeliene@ftmc.lt; arunas.tamasevicius@ftmc.lt

[b]Department of Physics, Vilnius Gediminas Technical University, Saulėtekio ave. 11, LT-10223 Vilnius, Lithuania
gytis.mykolaitis@vgtu.lt

Received: April 12, 2016 / **Revised:** October 12, 2016 / **Published online:** March 17, 2017

Abstract. Damping of spikes in an array of coupled oscillators by injection of sinusoidal current is studied both electronically and numerically. The effect is investigated using an array consisting of thirty mean-field coupled FitzHugh–Nagumo-type oscillators. The results are considered as a possible mechanism of the deep brain stimulation used to avoid the symptoms of the Parkinson's disease.

Keywords: coupled oscillators, FitzHugh–Nagumo oscillators, control of dynamical systems.

1 Introduction

Undesirable instabilities in dynamical systems can be avoided by applying conventional proportional feedback techniques [8, 11]. An example is a simple second-order system, where the proportional feedback is given by a linear term with a control coefficient k:

$$\dot{x} = F(x, y) + k(x^* - x), \qquad \dot{y} = G(x, y). \tag{1}$$

Here F and G are either linear or nonlinear functions, the x^* is a reference point, e.g. a steady state coordinate of the system. However, in many real systems, especially in biology, chemistry, physiology, etc., the exact locations of these states are unknown. Moreover, their positions may vary with time because of unknown and unpredictable forces. Therefore, adaptive methods, automatically tracing and stabilizing the steady states, are required. A large number of adaptive control techniques have been developed so far, e.g. the tracking filter method [9, 10, 15], and applied to a variety of dynamical systems (see [1, 19] and references therein). To implement the tracking filter technique, system (1)

should be provided with an additional equation describing the dynamical variable z of the first-order filter:

$$\dot{x} = F(x, y) + k(z - x), \qquad \dot{y} = G(x, y), \qquad \dot{z} = \omega_f(x - z), \tag{2}$$

where ω_f is the cut-off frequency of the filter (usually $\omega_f \ll 1$).

An alternative control method is a non-feedback technique based on applying to the system external periodic force:

$$\dot{x} = F(x, y) + A\sin(\omega t), \qquad \dot{y} = G(x, y). \tag{3}$$

In system (3), the frequency of the external forcing ω should be high enough in comparison with the natural frequency of the uncontrolled dynamical system. A specific example is the stabilization of the unstable upside-down position of a mechanical pendulum by vibrating its pivot up and down at a relatively high frequency [20]. Recently, this "mechanical" idea has been exploited in a seemingly unexpected field [12], namely, to get insight into the mechanism of the so-called deep brain stimulation (DBS) conventionally used for patients with the Parkinson's disease, essential tremor [2–4], and other brain malfunctions.

In this paper, we extend this research by demonstrating that external periodic forcing can inhibit spikes in an array of coupled neuronal oscillators. To be specific, we consider an array of the mean-field coupled electronic FitzHugh–Nagumo (FHN) oscillators, also known in literature as the Bonhoeffer–van der Pol oscillators [14].

2 Analogue circuits

The corresponding circuit diagrams are presented in Fig. 1. CN is a coupling node. It is assumed that the CN is not accessible directly from the outside, but via some passive resistance network represented here for simplicity by an equivalent resistance R_g. DN is an accessible damping node.

In Fig. 1(b), OA is a general-purpose operational amplifier, e.g. NE5534-type device, D_1 and D_2 are the BAV99-type Schottky diodes, $L = 10$ mH, $C = 3.3$ nF,

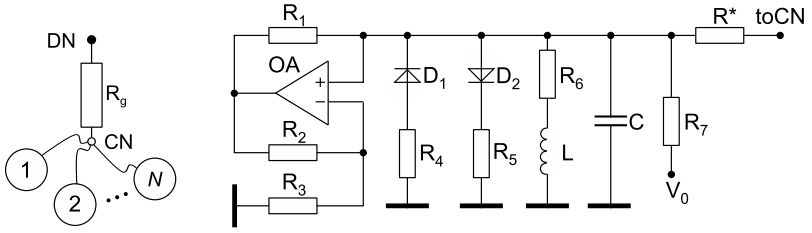

(a) (b)

Figure 1. Circuit diagrams: (a) array of mean-field coupled oscillators, (b) single asymmetric ($R_4 \ll R_5$) FHN-type oscillator.

$R_1 = R_2 = 1$ kΩ, $R_3 = 510\ \Omega$, $R_4 = 30\ \Omega$, $R_5 = 510\ \Omega$, $R_6 = 275\ \Omega$ (an external resistor $R'_6 = 220\ \Omega$ in series with the coil resistance $R''_6 = 55\ \Omega$), $R_{7i} = (24 + i)$ kΩ, $i = 1, 2, \ldots, N$, $R^* = 510\ \Omega$, $V_0 = -15$ V. The single FHN oscillator in Fig. 1(b) is a circuit with an asymmetric nonlinearity ($R_4 \ll R_5$). It is a slight modification of an oscillator described in [16] and essentially differs from the earlier asymmetric version of the FHN-type oscillator suggested in [5]. In the experiments, we employed a hardware array with $N = 30$ described in details (without any external control) elsewhere [17]. The external inhibitory current $I_{\rm inh}(t) = I_A \sin(2\pi f t)$ was injected from an external sine wave generator via the damping node DN.

3 Electronic experiments

In real neuronal systems, the typical spike parameters are the following: spike height is about 100 mV, spike width is about 1 ms, interspike interval ranges from several hundreds to several tens of milliseconds [7]. Consequently, the repetition rate f_0 of the spikes is from several Hz to several tens of Hz. Correspondingly, the practical DBS frequencies are chosen between 50 and 300 Hz [4]. Though an analog electronic circuit exhibiting the above neuron parameters, e.g. with f_0 =10 Hz, can be implemented as a hardware [18], in the present modelling experiment, we employed an array of FHN-type oscillators described in [17]. In this array, the frequencies of the individual units were intentionally set at 12 kHz, i.e. by about three orders higher than in real neurons. Such an increase of working frequency makes the analog experiment more convenient. All experimental data, in particular phase portraits, Poincaré sections, and power spectra can be taken on a real time scale [17]. Also, time averaging procedure of the signals become extremely fast.

For the best performance, it is necessary to choose an appropriate drive frequency f and amplitude I_A. The f should be much higher than the natural frequency f_0 of the spiking oscillators. The threshold value of the drive amplitude I_A^* depends on the frequency f. The I_A^* is relatively low in the interval from 50 to 500 kHz. Outside this range (below 50 and above 500 kHz), I_A^* increases rapidly. Similar amplitude–frequency dependence (a valley in a certain frequency range) was observed in real DBS experiments [3] with f from 100 until 5000 Hz, also for single electronic neuron model in low frequency experiment [18], where the optimal range of f was from 40 to about 400 Hz. In our present high frequency electronic experiments, we chose $f = 150$ kHz, i.e. in the middle between 50 and 500 kHz. The selected frequency provided the lowest threshold $I_A^* = 50$ mA.

The experimental results are shown in Figs. 2 and 3 by the waveforms and the phase portraits, respectively. Here the $\langle V_C \rangle$ is the mean-field voltage of the voltages V_{Ci} from the individual oscillators ($i = 1, 2, \ldots, 30$).

The time average of the high frequency non-spiking voltage $\langle V_C \rangle$ (right-hand side of the bottom plot), taken over the period ($T = 1/f$) of the external current, is $\bar{U}_C \approx -0.18$ V. It is non-zero value because of the DC bias V_0. The $\bar{U}_C$ is noticeably different from the natural steady state $\langle V_{0C} \rangle = -0.27$ V measured in a non-oscillatory mode (when the all coils L are short-circuited).

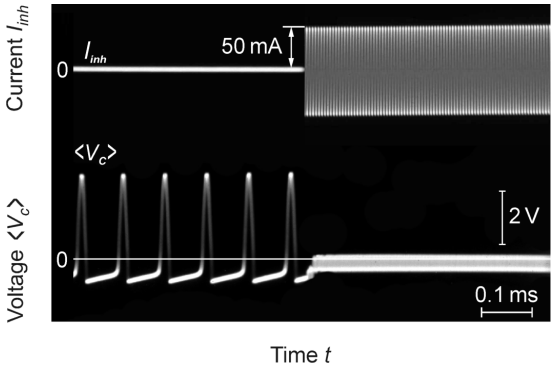

Figure 2. Experimental waveforms of the external periodic current $I_{\rm inh}$ and the mean-field voltage of the array $\langle V_C\rangle$; f=150 kHz.

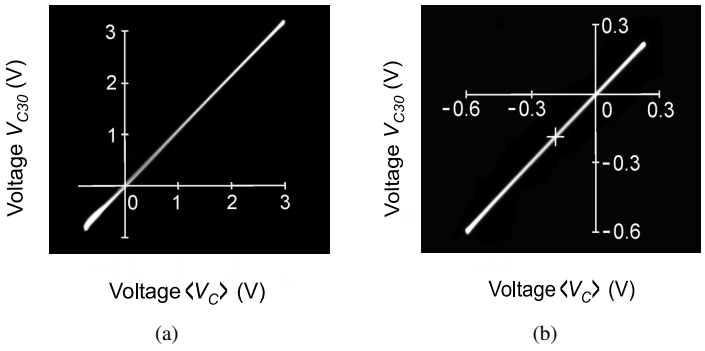

Figure 3. Phase portraits $[V_{C30}, \langle V_C\rangle]$: (a) spiking oscillators (no control, I_A = 0), (b) non-spiking oscillators, I_A = 50 mA, f = 150 kHz. Small cross in (b) marks the averages of the voltages $[\bar{U}_{C30}, \bar{U}_C]$ taken over the period of the external inhibitory current $I_{\rm inh}(t)$. They are at about $[-0.18$ V, -0.18 V]. Note different position of the diagonal, also different horizontal and vertical scales in (b) compared to (a).

Fine diagonals in Fig. 3, $[V_{C30},\ \langle V_C\rangle]$ indicate that the individual oscillator No. 30 is strongly synchronized with the mean-field of the array. Other oscillators, No. 1 to No. 29, were also checked experimentally by means of the phase portraits $[V_{Ci},\ \langle V_C\rangle]$ and gave similar result.

The self-sustained low frequency ($f_0 \approx 12$ kHz) spikes of about 3 V height are totally suppressed when the inhibitory current $I_A \geqslant I_A^* = 50$ mA is injected. However, we have a finite ($\approx 13\%$) higher frequency artefact. The voltage oscillates around the time average $\bar{U}_C$ with the amplitude of about 0.4 V at the external drive frequency f.

Moreover, the artefact voltage continues to change (Fig. 4) when the external drive amplitude I_A is increased above the threshold value I_A^* (the amplitude I_A should be higher than the threshold to guarantee robust inhibition). For example, at a double drive amplitude, $I_A/I_A^* = 2$ the average voltage changes its sign. Similar behaviour was observed earlier, but not emphasized in the numerically simulated bifurcation diagram for the Hodgkin–Huxley (HH) single neuron model [12].

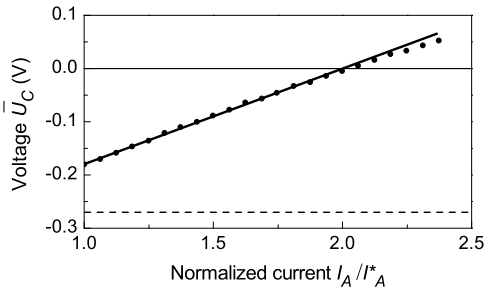

Figure 4. Time average of the mean-field voltage $\bar{U}_C$, taken over the period ($T = 1/f$) of the external inhibitory current $I_{\rm inh}$, as a function of the normalized amplitude I_A/I_A^* of the external current. $I_A^* = 50$ mA. Extrapolation to zero control ($I_A = 0$) provides a value of $\bar{U}_C$ close to the natural steady state $\langle V_{0C}\rangle = -0.27$ V (dashed line in the plot).

4 Mathematical model

Applying the Kirchhoff laws to the circuits in Fig. 1 with $R_1 = R_2$ and $R_7 \gg \max\{\sqrt{L/C}, R_3, R_4, R_5, R_6\}$, the following differential equations are derived:

$$\begin{aligned} C\frac{{\rm d}V_{Ci}}{{\rm d}t} &= \frac{V_{Ci}}{R_3} - I_D - I_{Li} + \frac{V_0}{R_{7i}} + \frac{\langle V_C\rangle - V_{Ci}}{R^*} + \frac{I_A\sin(2\pi ft)}{N}, \\ L\frac{{\rm d}I_{Li}}{{\rm d}t} &= V_{Ci} - R_6 I_{Li}, \quad i = 1, 2, \ldots, N. \end{aligned} \tag{4}$$

The nonlinear current–voltage (I–V) characteristic $I_D = I_D(V_{Ci})$ of the D_1R_4–D_2R_5 composite in system (4) is approximated by three segments of linear functions

$$I_D(V_{Ci}) = \begin{cases} (V_{Ci} + V^*)/R_4, & V_{Ci} < -V^*, \\ 0, & -V^* \leqslant V_{Ci} \leqslant V^*, \\ (V_{Ci} - V^*)/R_5, & V_{Ci} > V^*. \end{cases}$$

Here V^* is the breakpoint voltage of the forward I–V characteristic of the diodes ($V^* \approx 0.6$ V). In system (4), the individual oscillators are coupled via the mean-field voltage

$$\langle V_C\rangle = \frac{1}{N}\sum_{i=1}^{N} V_{Ci}. \tag{5}$$

We introduce the following set of dimensionless variables and parameters:

$$\begin{aligned} &x_i = \frac{V_{Ci}}{V^*}, \quad y_i = \frac{\rho I_{Li}}{V^*}, \quad t \to \frac{t}{\sqrt{LC}}, \quad \langle x\rangle = \frac{1}{N}\sum_{i=1}^{N} x_i, \\ &\rho = \sqrt{\frac{L}{C}}, \quad a = \frac{\rho}{R_3}, \quad b = \frac{R_6}{\rho}, \quad c_i = \frac{\rho V_0}{R_{7i}V^*}, \\ &d_1 = \frac{\rho}{R_4}, \quad d_2 = \frac{\rho}{R_5}, \quad k = \frac{\rho}{R^*}, \end{aligned} \tag{6}$$

also, two additional dimensionless parameters for the external sine wave forcing:

$$A = \frac{\rho I_A}{NV^*}, \qquad \omega = 2\pi f\sqrt{LC}, \tag{7}$$

and we arrive to a set of $2N$ coupled non-autonomous differential equations convenient for numerical integration:

$$\begin{aligned} \dot{x_i} &= ax_i - f(x_i) - y_i + c_i + k\big(\langle x\rangle - x_i\big) + A\sin(\omega t),\\ \dot{y_i} &= x_i - by_i, \quad i = 1, 2, \ldots, N. \end{aligned} \tag{8}$$

The $f(x_i)$ in system (8) is a nonlinear function presented by a piecewise linear function

$$f(x_i) = \begin{cases} d_1(x_i + 1), & x_i < -1,\\ 0, & -1 \leqslant x_i \leqslant 1,\\ d_2(x_i - 1), & x_i > 1. \end{cases}$$

Note that, due to $d_1 \gg d_2$, the $f(x_i)$ is an essentially asymmetric function [16] in contrast to the common FHN cubic parabola x^3 introduced by FitzHugh [6]. The DC bias parameters c_i are intentionally set different for each individual oscillator, thus making them non-identical units.

5 Numerical results

Integration of system (8) has been performed using the Wolfram Mathematica package. The numerical results are presented in Fig. 5. They are in a good agreement with the experimental plots in Fig. 2. The mean-field variable $\langle x\rangle$ does not converge to a constant steady state, but oscillates around it at the drive frequency. Strictly speaking, the non-autonomous (externally driven) dynamical systems, e.g. given by system (8), do not possess steady states at all. Only in the case of high frequency ($f \gg f_0$) drive, we can introduce the average values taken over the external period. These averages are related to the real steady states.

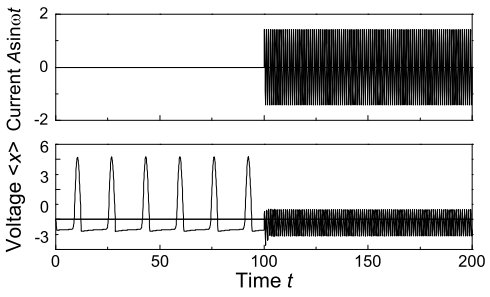

Figure 5. Simulated waveforms of the inhibitory current $A\sin(\omega t)$ and the mean-field voltage $\langle x\rangle$ from system (8); $N = 30$. $A = 5.1$, $\omega = 6.28$, $a = 3.4$, $b = 0.16$, $c_i = -44/(24 + i)$, $i = 1, 2, \ldots, 30$, $d_1 = 60$, $d_2 = 3.4$, $k = 3.4$. The external inhibitory term $A\sin(\omega t)$ is activated at $t = 100$.

6 Mean-field approach

Analysis of system (8) can be essentially simplified if we consider only the mean-field variables obtained by the direct averaging of x_i, y_i, $f(x_i)$, $k(\langle x\rangle - x_i)$, and c_i in the original equations:

$$\begin{aligned} \langle \dot{x}\rangle &= a\langle x\rangle - \big\langle f(x_i)\big\rangle - \langle y\rangle + \langle c\rangle + A\sin(\omega t),\\ \langle \dot{y}\rangle &= \langle x\rangle - b\langle y\rangle. \end{aligned} \tag{9}$$

As a result, the mean of the coupling term $\langle k(\langle x\rangle - x_i)\rangle = k(\langle x\rangle - \langle x\rangle) = 0$ in system (9) has been nullified independently on the value of k. Further, we assume that all $|x_i| \leqslant 1$. According to definition of the nonlinear function $f(x_i)$, this leads to $f(x_i) = \langle f(x_i)\rangle = 0$. Eventually, we obtain a set of linear differential equations, which do not describe the full dynamics of the mean field, but provide its steady state. In the absence of the external drive ($A = 0$), it has the following coordinates (for $ab < 1$ and $|c_i| \leqslant 1/b - a$):

$$\langle x_0\rangle = \frac{b\langle c\rangle}{1-ab}, \qquad \langle y_0\rangle = \frac{\langle c\rangle}{1-ab}. \tag{10}$$

Stability analysis of system (9) shows that, for A = 0 and $a > b$, the steady state is unstable (the real parts of the both eigenvalues of the corresponding second-order characteristic equation are both positive). If (in addition to $a > b$) the sum $a + b > 2$, then the eigenvalues are real (no imaginary parts). Thus, the steady state is an unstable node. Whereas the external periodic forcing ($A \neq 0$), similarly to the mechanical pendulum [20] and the single HH neuron [12], stabilizes the originally unstable steady state.

For the parameter values employed in numerical simulations: $a = 3.4$, $b = 0.16$, and $c_i = -44/(24 + i)$, the steady-state coordinates have the following numerical values: $x_0 = -0.41$, $y_0 = -2.57$. Using the definitions of the dimensionless variables introduced in (6), we estimate the means of the steady-state coordinates of the original system: $\langle V_{0C}\rangle \approx -0.25$ V, $\langle I_{0L}\rangle \approx -1$ mA. The estimated steady-state voltage $\langle V_{0C}\rangle$ is close to its experimental value -0.27 V.

7 Conclusions

The recent papers [12, 13] on suppression of neuronal spikes by means of periodic force consider mathematical models of single neurons. Our paper [16] on an adaptive feedback technique for damping neuronal activity also deals with a single oscillator only. The present work extends the above investigations to an array of coupled (synchronized) neuronal oscillators. In addition to numerical simulations, we have carried out a hardware experiment using an analog electronic network described in [17]. This research can serve for better understanding the mechanism of the DBS technique.

The influence of strongly perturbed steady states of the neurons on the effectiveness of DBS technique has not been investigated yet. However, one can suppose that the high frequency artefact oscillations (Fig. 2) and especially its unnatural DC component (Fig. 4) probably can cause the undesirable side effects in the real neuronal systems.

References

1. E. Adomaitienė, G. Mykolaitis, S. Bumelienė, A. Tamaševičius, Adaptive nonlinear controller for stabilizing saddle steady states of dynamical systems, *Nonlinear Dyn.*, **82**(4):1743–1753, 2015.
2. A.L. Benabid, S. Chabardes, J. Mitrofanis, P. Pollak, Deep brain stimulation of the subthalamic nucleus for the treatment of Parkinson's disease, *Lancet Neurol.*, **8**(1):67–81, 2009.
3. A.L. Benabid, P. Pollak, C. Gervason, D. Hoffman, D.M. Gao, M. Hommel, J.E. Perret, J. de Rougemont, Long-term suppression of tremor by chronic stimulation of the ventral intermediate thalamic nucleus, *Lancet*, **337**:403–406, 1991.
4. A.L. Benabid, P. Pollak, A. Louveau, S. Henry, J. de Rougemont, Combined (thalamotomy and stimulation) stereotactic surgery of the vim thalamic nucleus for bilateral Parkinson disease, *Appl. Neurophysiol.*, **50**:344–346, 1987.
5. S. Binczak, V.B. Kazantsev, V.I. Nekorkin, J.M. Bilbaut, Experimental study of bifurcations in modified FitzHugh–Nagumo cell, *Electron. Lett.*, **39**(13):961–962, 2003.
6. R. FitzHugh, Impulses and physiological states in theoretical models of nerve membrane, *Biophys. J.*, **1**(6):445–466, 1961.
7. W. Gerstner, W. Kistler, *Spiking Neuron Models*, Cambridge University Press, Cambridge, 2005.
8. B.C. Kuo, *Automatic Control Systems*, Prentice Hall, Englewood Cliffs, NJ, 1995.
9. A. Namajūnas, K. Pyragas, A. Tamaševičius, Stabilization of an unstable steady state in a Mackey–Glass system, *Phys. Lett. A*, **204**(2):255–262, 1995.
10. A. Namajūnas, K. Pyragas, A. Tamaševičius, Analog techniques for modeling and controlling the Mackey–Glass system, *Int. J. Bifurcation Chaos Appl. Sci. Eng.*, **7**(4):957–962, 1997.
11. K. Ogata, *Solvability of Nonlinear Equations and Boundary Value Problems*, Prentice Hall, Englewood Cliffs, NJ, 2010.
12. K. Pyragas, V. Novičenko, P.A. Tass, Mechanism of suppression sustained neuronal spiking under high-frequency stimulation, *Biol. Cybern.*, **107**:669–684, 2013.
13. A. Rabinovitch, Y. Biton, D. Braunstein, M. Friedman, I. Aviram, A neuron under external sinusoidal stimulation, *Brain Stimulation*, **8**:310–325, 2015.
14. A. Rabinovitch, R. Thieberger, M. Friedman, Forced Bonhoeffer–van der Pol oscillator in its excited mode, *Phys. Rev. E*, **50**(2):1572–1578, 1994.
15. N.F. Rulkov, L.S. Tsimring, H.D.I. Abarbanel, Tracking unstable orbits in chaos using dissipative feedback control, *Phys. Rev. E*, **50**:314–324, 1994.
16. A. Tamaševičius, E. Tamaševičiūtė, G. Mykolaitis, S. Bumelienė, R. Kirvaitis, R. Stoop, Neural spike suppression by adaptive control of an unknown steady state, in C. Alippi, M. Polycarpou, C. Panayiotou, G. Ellinas (Eds.), *Artificial Neural Networks – ICANN 2009, 19th International Conference, Limassol, Cyprus, September 14–17, 2009, Proceedings, Part I*, Lect. Notes Comput. Sci., Vol. 5768, Springer, Berlin, Heidelberg, 2009, pp. 618–627.
17. E. Tamaševičiūtė, G. Mykolaitis, A. Tamaševičius, Analogue modelling an array of the FitzHugh–Nagumo oscillators, *Nonlinear Anal. Model. Control*, **17**(1):118–125, 2012.

18. E. Tamaševičiūtė, G. Mykolaitis, A. Tamaševičius, 'Realistic' electronic neuron, in *Proceedings of 2012 International Symposium on Nonlinear Theory and its Applications (NOLTA2012), Palma, Majorca, Spain, October 22–26, 2012*, IEICE, Tokyo, 2012, pp. 860–863.

19. E. Tamaševičiūtė, A. Tamaševičius, G. Mykolaitis, S. Bumelienė, Tracking and controlling unstable steady states of dynamical systems, *Commun. Nonlinear Sci. Numer. Simul.*, **19**(3):649–655, 2014.

20. J.J. Thomsen, *Vibrations and Stability – Advanced Theory, Analysis and Tools*, Springer, Berlin, Heidelberg, New York, 2003.